Isolas versus snaking of localized rolls

Tarik Aougab[1], Margaret Beck[2], Paul Carter[3], Surabhi Desai[4], Björn Sandstede[5], Melissa Stadt[6],
and Aric Wheeler[7]

[1]Department of Mathematics, Brown University, Providence, RI, USA
[2]Department of Mathematics and Statistics, Boston University, Boston, MA, USA
[3]Department of Mathematics, University of Arizona, Tucson, AZ, USA
[4]Mathematical Institute, University of St Andrews, St Andrews, Scotland
[5]Division of Applied Mathematics, Brown University, Providence, RI, USA
[6]Department of Mathematics, University of Washington, Seattle, WA, USA
[7]Department of Mathematics, University of North Carolina, Chapel Hill, NC, USA

October 5, 2017

Abstract

We analyze the bifurcation diagrams of spatially localized stationary patterns that exhibit a long spatially periodic interior plateau (referred to as localized rolls). In a wide variety of contexts, these bifurcation diagrams consist of isolas or of intertwined s-shaped curves that are commonly referred to as snaking branches. These diagrams have been rigorously analyzed by connecting the existence curves of localized rolls with the bifurcation structure of fronts that connect the rolls to the trivial state. Previous work assumed that the stable and unstable manifolds of rolls were orientable. Here, we extend these results to the nonorientable case and also discuss topological barriers that prevent snaking, thus allowing only isolas to occur. The results are applied to the Swift–Hohenberg system for which we show that nonorientable roll patterns cannot snake.

1 Introduction

A wide variety of physical systems support stationary spatially localized patterns, or localized rolls, that exhibit a bifurcation structure known as snaking (see, for instance, [3, 4, 9, 11]). In one spatial dimension, such solutions have a region of finite length, say $2L$, in the interior of the domain where they are essentially spatially periodic, and then decay to the background rest state exponentially fast outside of that region: Figure 1 shows an example of a symmetric localized pattern. The snaking bifurcation diagram is typically characterized by a pair of curves that wind back and forth as they extend vertically upward when they are plotted as a function of a bifurcation parameter, say μ, against some measure of the size of the pattern, which is typically the L^2 norm but can be intuitively thought of as L. These curves are often accompanied by horizontal branches that correspond to accompanying asymmetric localized patterns of corresponding length (see Figure 1). Due to the ubiquity of this phenomenon in seemingly disparate physical models, a significant effort was made to explain snaking bifurcations mathematically. This work builds upon that effort, and in particular on the results in [2]. There, the authors were able to analyze snaking by viewing the localized patterns as being composed of fronts and backs that connect the rolls to the trivial state (see Figure 2) and using assumptions about the structure of certain stable and unstable manifolds associated with the fronts and backs to deduce the existence of snaking. The main goal of this paper is to conduct a similar analysis in
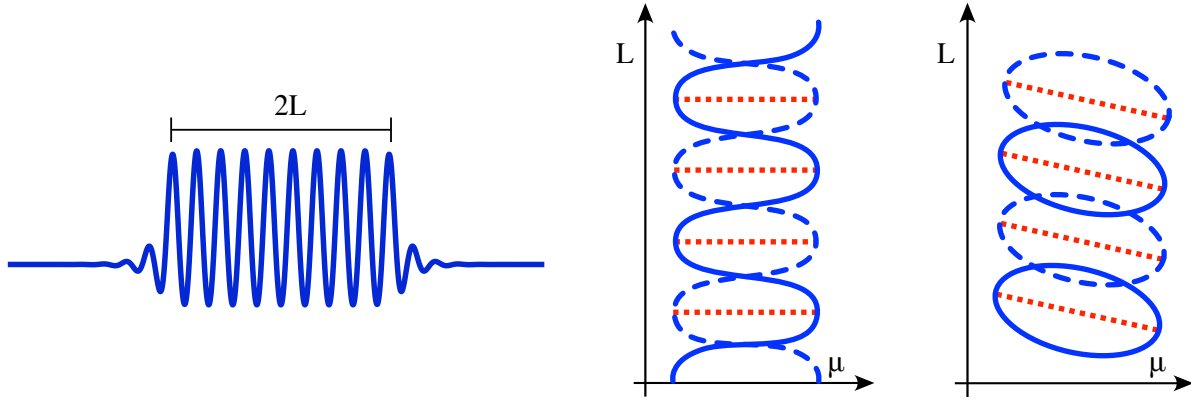
Figure 1: *Shown are the graph of a localized pattern with a roll plateau of length 2L as a function of space x [left panel] and schematic depictions of bifurcation diagrams that exhibit snaking [center panel] and disconnected closed curves (or isolas) [right panel]: in the rightmost two panels, the solid and dashed curves correspond to the separate branches of symmetric pulses that have, respectively, a minimum and a maximum at their center, while the dotted curves correspond to disconnected branches of asymmetric pulses. Note that, throughout the paper, we will not indicate PDE stability in our bifurcation diagrams.*
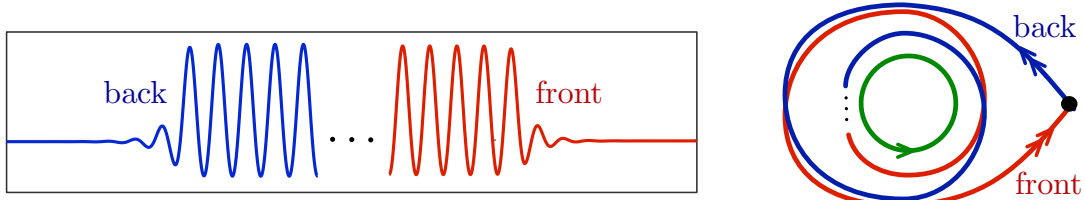

Figure 2: *The left panel shows the graphs of a back and a front as functions of space x. The interpretation of these patterns as heteroclinic orbits connecting the rest state to a periodic orbit is shown in the right panel. These heteroclinic solutions can be glued together to form a homoclinic orbit to the rest state that spends much of its trajectory near the periodic orbit, thus corresponding to a localized roll patterns.*

the case where those stable and unstable manifolds are nonorientable and to determine to what extent snaking is still possible in this case.

A concrete system that exhibits snaking is the Swift–Hohenberg equation

$$U_t = -(1 + \partial_x^2)^2 U - \mu U + \nu U^2 - U^3, \qquad x \in \mathbb{R}, \tag{1.1}$$

where $\nu > 0$ is kept fixed and $\mu > 0$ serves as the bifurcation parameter. The condition $\mu > 0$ ensures that the background state $U = 0$ is stable. Stationary solutions of (1.1) satisfy an equation of the form

$$u_x = f(u, \mu), \qquad u = (U, U_x, U_{xx}, U_{xxx}) \in \mathbb{R}^4, \tag{1.2}$$

which has the conserved quantity

$$H(u, \mu) = u_2 u_4 - \frac{1}{2} u_3^2 + u_2^2 + \frac{(1+\mu)}{2} u_1^2 - \frac{\nu}{3} u_1^3 + \frac{1}{4} u_1^4.$$

The presence of the conserved quantity allows us to restrict attention to the three-dimensional zero level set of H. System (1.2) is also reversible and possesses a family of periodic orbits denoted by $\gamma(x, \mu)$ that are contained in the zero level set of H. The fronts and back in Figure 2 can be viewed as heteroclinic connections between $u = 0$ and the periodic orbits $\gamma(x, \mu)$, and the localized patterns are homoclinic orbits that connect $u = 0$ to itself and spend some amount of time (determined by L) near the periodic orbits; see Figure 2. We note that our results will apply to any system of the form (1.2) in $\mathbb{R}^4$, not just to that associated with stationary solutions of (1.1), as long as it
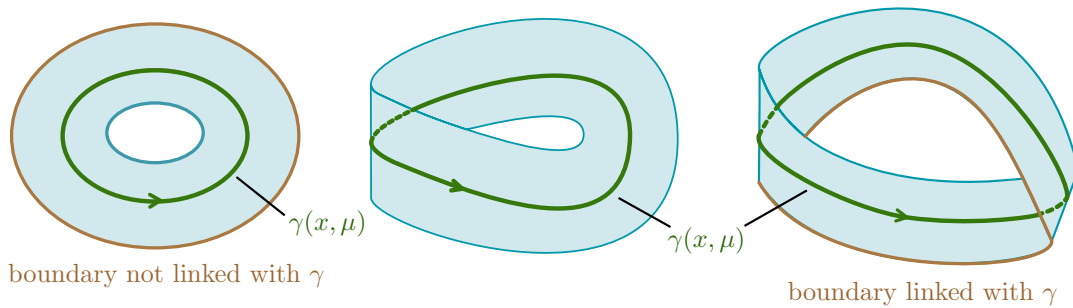
Figure 3: *Shown are the periodic orbit $\gamma(x, \mu)$ and its two-dimensional unstable manifold within the three-dimensional zero level set of the energy. The three panels indicate the cases where, from left to right, the unstable manifold is orientable without twist (thus homeomorphic to a cylinder), nonorientable with a half twist (hence homeomorphic to a Möbius band), and orientable with a full twist (again homeomorphic to a cylinder). Note that, in contrast to the case without twist, the boundary of the rightmost unstable manifold forms a nontrivial knot with the periodic orbit.*

satisfies the hypotheses in §2 and §3. We note that other works have considered the effects of removing some of the assumptions such as reversibility or the existence of conserved quantities [6–8, 10].

A key assumption of [2] was that the nontrivial Floquet multipliers of the periodic orbits γ are positive, which implies that the two-dimensional stable and unstable manifolds of γ are orientable, and therefore topological cylinders; see Figure 3. In this case, depending on how the two-dimensional unstable manifold of the periodic orbits γ intersect the two-dimensional stable manifold of the rest state $u = 0$ within the three-dimensional zero level set of the energy H, the resulting bifurcation diagram of localized rolls either exhibits snaking or consists of infinitely many disconnected closed curves (from now on referred to as isolas) as indicated in Figure 1. We remark that the difference between snaking and isolas is visible only through the structure of the bifurcation diagram (and, specifically, boundedness and connectedness of branches in the (μ, L)-plane): in particular, numerical continuation methods can distinguish between these cases, but direct simulations are, in general, not capable of differentiating between them.

In this paper, we consider the case where the unstable manifolds of the periodic orbits are nonorientable, thus topologically taking the form of Möbius bands. We also consider more general twisting, e.g. an orientable surface with full twist; see Figure 3 for an illustration. Due to the fact that the phase space is not $\mathbb{R}^3$, but rather a three dimensional submanifold of $\mathbb{R}^4$ given by the zero level set $H^{-1}(0)$ of the conserved quantity H, this general notion of twisting must be defined relative to the topology of $H^{-1}(0)$. We will show that the geometric structure of a certain set Γ that captures the existences of fronts and backs between the origin and the roll patterns determines whether the bifurcation branches of symmetric localized rolls consist of isolas or of snaking branches. We will also show that the topological structure of the zero level set of the conserved quantity can impose topological barriers for snaking: more specifically, twisting as described above can cause linking of unstable manifolds with the underlying periodic orbit and prevent snaking by restricting the possibilities for the geometric configuration of the set Γ. In particular, we will show that rolls with nonorientable or more generally twisted unstable manifolds cannot lead to snaking branches in the Swift–Hohenberg equation. We note that the nonorientable case was considered previously in a related scenario in [6], but it was assumed there that the set Γ that captures how the strong unstable fibers of the periodic orbit intersect the stable manifold of the homogeneous rest state could be represented as a graph: we will show in this work that this hypothesis on Γ is not compatible with the nonorientability assumption.

The rest of the paper is organized as follows. In §2, we collect the hypotheses and results from [2] for systems with orientable manifolds. In §3, we extend the framework from [2] to nonorientable manifolds and use the extended framework in §4 to provide conditions that lead to the existence of snaking and isolas of symmetric pulses as well as branches of asymmetric pulses. In §5, we then introduce a topological requirement that is necessary for the snaking conditions of §4 to hold. We show in §6 that this requirement is not satisfied for periodic orbits with twisted Floquet bundles in the Swift–Hohenberg equation and demonstrate numerically that indeed only isolas occur in this case.

We conclude with a discussion in §7.

2   Setup for positive Floquet multipliers

In this section, we summarize the hypotheses and results from [2] for the orientable case that will be used in later sections. Consider the ordinary differential equation

$$u_x = f(u, \mu), \quad u \in \mathbb{R}^4, \quad \mu \in \mathbb{R}, \tag{2.1}$$

where f is some smooth function. Since we are interested in reversible systems, assume the following hypothesis.

Hypothesis 1. *There exists a linear map* $\mathcal{R} : \mathbb{R}^4 \to \mathbb{R}^4$ *with* $\mathcal{R}^2 = 1$ *and* $\dim \text{Fix} \, \mathcal{R} = 2$, *where* $\text{Fix} \, \mathcal{R}$ *is the set of fixed points of* $\mathcal{R}$, *so that* $f(\mathcal{R}u, \mu) = -\mathcal{R}f(u, \mu)$ *for all* (u, μ).

It follows readily from Hypothesis 1 that the function $\tilde{u}(x) = \mathcal{R}u(-x)$ satisfies (2.1) whenever $u(x)$ does. We say a solution $u(x)$ is symmetric whenever $u(x) = \mathcal{R}u(-x)$ or, equivalently, whenever $u(0) \in \text{Fix} \, \mathcal{R}$. Next, we assume that the origin is a hyperbolic equilibrium for all values of μ.

Hypothesis 2. *The origin* $u = 0$ *is a hyperbolic equilibrium of* (2.1). *Furthermore,* $f_u(0, \mu)$ *has two eigenvalues with strictly negative real part and two eigenvalues with strictly positive real part.*

Note that the assumption on the spectrum is generic as Hypothesis 1 implies that the spectrum of $f_u(0, \mu)$ is invariant under multiplication by -1. To see this, note that $\mathcal{R}f(u, \mu) = -f(\mathcal{R}u, \mu)$ implies $\mathcal{R}f_u(u, \mu) = -f_u(\mathcal{R}u, \mu)\mathcal{R}$. Multiplying by $\mathcal{R}^{-1}$ from the right, we arrive at

$$\mathcal{R}f_u(u, \mu)\mathcal{R}^{-1} = -f_u(\mathcal{R}u, \mu) \quad \text{or, equivalently,} \quad -\mathcal{R}f_u(\mathcal{R}u, \mu)\mathcal{R}^{-1} = f_u(u, \mu) \qquad \text{for all } u \in \mathbb{R}^4 \tag{2.2}$$

and substituting $u = 0$ into the first equation proves our claim. Our next assumption deals with the existence of a conserved quantity that is invariant under the reverser $\mathcal{R}$.

Hypothesis 3. *There is a smooth function* $H : \mathbb{R}^4 \times \mathbb{R} \to \mathbb{R}$ *with* $H(\mathcal{R}u, \mu) = H(u, \mu)$ *and* $\langle H_u(u, \mu), f(u, \mu) \rangle = 0$ *for all* (u, μ). *We normalize* H *so that* $H(0, \mu) = 0$ *for all* μ.

We next assume that, for each μ in an appropriate interval, (2.1) has a symmetric periodic orbit in the zero energy level set $H^{-1}(0)$. The term "periodic orbit" will be used for solutions with nonzero minimal period.

Hypothesis 4. *We assume that there is a closed interval* $J \subset \mathbb{R}$ *with nonempty interior* $\overset{\circ}{J}$ *so that* (2.1) *has, for each* $\mu \in J$, *a periodic orbit* $\gamma(x, \mu)$ *with nonzero minimal period* $\ell(\mu)$ *which satisfies the following:*

  (i) *The family* $\gamma(x, \mu)$ *depends smoothly on* $\mu \in J$;
  (ii) $\gamma(x, \mu)$ *is symmetric:* $\gamma(0, \mu) \in \text{Fix} \, \mathcal{R}$ *for all* $\mu \in J$;
  (iii) $\gamma(x, \mu)$ *has zero energy: for each* $\mu \in J$, $H(\gamma(x, \mu), \mu) = 0$ *and* $H_u(\gamma(x, \mu), \mu) \neq 0$ *for one, and hence all,* x.
  (iv) $\gamma(x, \mu)$ *is hyperbolic (so has precisely two Floquet multipliers at one, and no others on the unit circle).*

Rescaling time appropriately, we can assume without loss of generality that all the minimal periods $\ell(\mu)$ are equal to 2π so that we can parametrize the periodic orbits by their phase $\varphi \in S^1 := [0, 2\pi]/\sim$. Next, consider the variational equation

$$v_x = f_u(\gamma(x, \mu), \mu)v \tag{2.3}$$

about $\gamma(x, \mu)$. Reversibility implies the following proposition.

Proposition 2.1. *If* $v(x)$ *satisfies* (2.3), *so does* $\tilde{v}(x) = \mathcal{R}v(-x)$. *In particular, whenever* (2.3) *has a solution of the form* $v(x) = e^{\alpha x}p(x)$ *for some* $\alpha \in \mathbb{C}$ *and some nonzero* 2π-*periodic function* $p(x)$, *then* $\tilde{v}(x) = e^{-\alpha x}\tilde{p}(x)$ *with* $\tilde{p}(x) := \mathcal{R}p(-x)$ *also satisfies* (2.3): *in particular, if* α *is a Floquet exponent, so is* $-\alpha$.
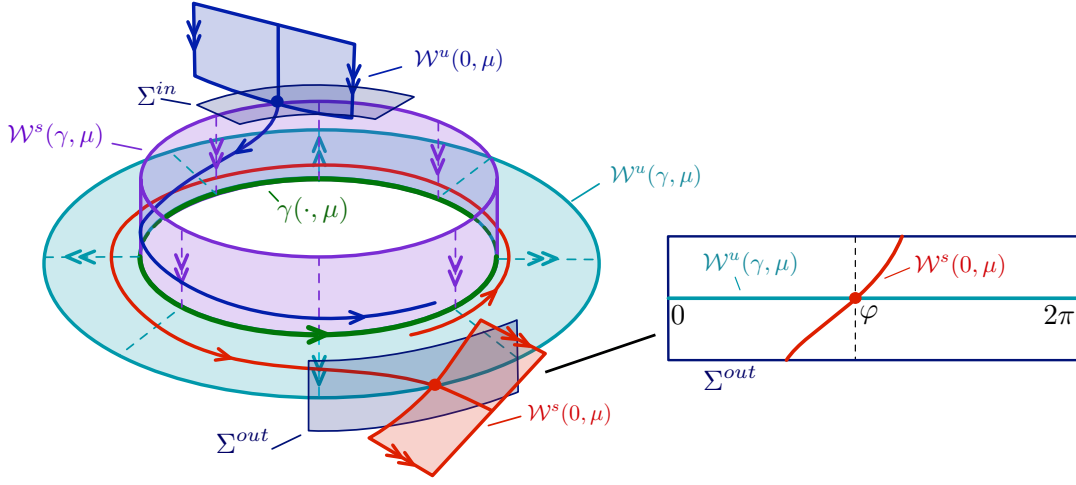
4

Figure 4: *Shown is a schematic of the geometry and the gluing construction near a periodic orbit with orientable stable and unstable manifolds without twists within the three-dimensional energy level set. Also shown are backs and fronts that correspond to intersections of $W^u(0, \mu)$ with $W^s(\gamma(x, \mu), \mu)$ and $W^s(0, \mu)$ with $W^u(\gamma(x, \mu), \mu)$, respectively, and a zoom-in of the section Σ^{out}. Note that the sections Σ_{in} and Σ_{out} actually traverse all the way around the cylinders, but this is not drawn for clarity.*

Proof. Let $v(x)$ be a solution to (2.3) and define $\tilde{v}(x) := \mathcal{R}v(-x)$. We then have

$$\tilde{v}_x(x) = -\mathcal{R}v_x(-x) \stackrel{(2.3)}{=} -\mathcal{R}f_u(\gamma(-x, \mu), \mu)v(-x) = -\mathcal{R}f_u(\mathcal{R}\gamma(x, \mu), \mu)\mathcal{R}^{-1}\mathcal{R}v(-x) \stackrel{(2.2)}{=} f_u(\gamma(x, \mu), \mu)\tilde{v}(x),$$

and we conclude that $\tilde{v}(x)$ also satisfies (2.3). The remaining claim follows immediately. $\qquad\square$

The preceding proposition implies that, whenever $\alpha \in \mathbb{C}$ is a Floquet exponent of $\gamma(x, \mu)$, then so is $-\alpha$. Our next hypothesis assumes that the nontrivial Floquet multipliers of the periodic orbits $\gamma(x, \mu)$ are positive or, equivalently, that the nontrivial Floquet exponents are real (and negatives of each other by Proposition 2.1).

Hypothesis 5. *$\gamma(x, \mu)$ has two positive nontrivial Floquet multipliers $\mathrm{e}^{\pm 2\pi\alpha(\mu)}$ with $\alpha(\mu) > 0$ for all $\mu \in J$.*

Consider the variational equation (2.3) about $\gamma(x, \mu)$. Due to Hypothesis 5, it has two nontrivial solutions v^s and v^u of the form

$$v^s(x) = \mathrm{e}^{-\alpha(\mu)x}p^s(x, \mu), \qquad v^u(x) = \mathrm{e}^{\alpha(\mu)x}p^u(x, \mu), \qquad \alpha(\mu) > 0, \tag{2.4}$$

where $p^s(x, \mu)$ and $p^u(x, \mu)$ are real valued and 2π-periodic in x. Proposition 2.1 implies that we can set $p^u(x, \mu) := \mathcal{R}p^s(-x, \mu)$ for all x and $\mu \in J$. In particular, the local stable and unstable manifolds $W^s(\gamma(x, \mu), \mu)$ and $W^u(\gamma(x, \mu), \mu)$ of the periodic orbits are diffeomorphic to an annulus as illustrated in Figure 4, and we will therefore refer to this case as the orientable case.

In [2], Fenichel coordinates were used locally to straighten out the strong stable and unstable fibers of γ, which results in a coordinate system of the form

$$\hat{v} = (\hat{v}^c, \hat{v}^s, \hat{v}^u) \in \mathcal{V} := S^1 \times I \times I, \qquad I = [-\delta, \delta]$$

near the periodic orbits. In these coordinates, $\hat{v}^c$ corresponds to the phase along the periodic orbit, and the sets $\{\hat{v}^u = 0\}$ and $\{\hat{v}^s = 0\}$ correspond to the stable and unstable manifolds of the periodic orbit, respectively. Furthermore, the strong unstable fiber $W^{uu}(\gamma(\varphi, \mu), \mu)$ of the point $\gamma(\varphi, \mu)$ on the periodic orbit corresponds to the set $\{\hat{v} : \hat{v}^c = \varphi, \hat{v}^s = 0\}$ and analogously for the strong stable fibers. In these coordinates, we can then define the sections Σ_{out} and Σ_{in} by

$$\Sigma_{\mathrm{in}} = S^1 \times \{\hat{v} : \hat{v}^s = \delta\} \times I, \qquad \Sigma_{\mathrm{out}} = S^1 \times I \times \{\hat{v} : \hat{v}^u = \delta\}.$$

As indicated in Figure 4, generically, $W^s(0, \mu)$ will intersect Σ_{out} in a one-dimensional curve, and intersections of $W^s(0, \mu)$ with $W^u(\gamma(x, \mu), \mu)$ correspond to front solutions. These intersections are encoded in the set

$$\Gamma := \{(\varphi, \mu) \in S^1 \times J : W^s(0, \mu) \cap W^{uu}(\gamma(\varphi, \mu), \mu) \cap \Sigma_{\text{out}} \neq \emptyset\}$$

that keeps track of the specific unstable fibers in which the fronts lie. In [2], it was shown that the global structure of the bifurcation diagrams of localized patterns can be deduced entirely from the structure of the set Γ. In particular, under some mild nondegeneracy conditions, it was shown that snaking of symmetric pulses will occur whenever Γ can be represented as a graph $\mu = z(\varphi)$ for $\varphi \in S^1$: note that this requires that, for each fixed phase φ, there is a parameter value μ for which the strong unstable finger of $\gamma(\varphi, \mu)$ intersects the stable manifold of the origin. In §5, we will show that the set Γ cannot be represented as a graph when the stable and unstable manifolds of γ are nonorientable or, more generally, twisted.

When Γ cannot be represented as a graph over S^1, other bifurcation diagrams can arise. In particular, it was shown in [2] that the bifurcation diagram can consist of a sequence of disconnected closed curves, or isolas, comprised of symmetric localized patterns that spend arbitrarily long times near the periodic orbit γ. We show in §4 that this behavior can also occur regardless of twisting.

3 Setup for negative Floquet multipliers

We now consider the case of negative Floquet multipliers. We assume that Hypotheses 1-4 that we stated in §2 and that were used in [2] are met, but replace Hypothesis 5 with the following assumption:

Hypothesis 6. *The periodic orbits $\gamma(x, \mu)$ have two nontrivial negative Floquet multipliers $e^{\pm 2\pi(\alpha(\mu)+i/2)} = -e^{\pm 2\pi\alpha(\mu)}$ with $\alpha(\mu) > 0$ for each $\mu \in J$.*

Note that Proposition 2.1 implies that Floquet exponents come in pairs, related by multiplication by -1. The primary outcome of Hypothesis 6 is that the stable and unstable manifolds of $\gamma(x, \mu)$ are topologically Möbius bands. To see this, we first state the following lemma.

Lemma 3.1. *Assume that Hypotheses 1-4 and 6 are met. The variational equation*

$$v_x = f_u(\gamma(x, \mu), \mu)v \tag{3.1}$$

then has two nontrivial solutions $v^s(x)$ and $v^s(x)$ of the form

$$v^s(x) = e^{-\alpha(\mu)x}p^s(x, \mu), \qquad v^u(x) = e^{\alpha(\mu)x}p^u(x, \mu) = e^{\alpha(\mu)x}\mathcal{R}p^s(-x, \mu), \qquad \alpha(\mu) > 0, \tag{3.2}$$

where $p^s(x, \mu)$ and $p^u(x, \mu)$ are real valued, 4π-periodic in x, and satisfy

$$p^s(x + 2\pi, \mu) = -p^s(x, \mu), \qquad p^u(x + 2\pi, \mu) = -p^u(x, \mu) \tag{3.3}$$

for all x and $\mu \in J$.

Proof. Using Floquet theory, Hypothesis 6 implies that the variational equation (3.1) has a nontrivial solution of the form $v(x) = e^{-(\alpha(\mu)+i/2)x}p(x, \mu)$, where $\alpha(\mu) > 0$ and the complex-valued function $p(x, \mu)$ satisfies $p(x + 2\pi, \mu) = p(x, \mu)$ for all x. We set

$$p^s(x, \mu) := \text{Re}\left(e^{-ix/2}p(x, \mu)\right)$$

so that $p^s(x + 2\pi, \mu) = -p^s(x, \mu)$ and $p^s(x + 4\pi, \mu) = p^s(x, \mu)$ for all x, and conclude that the function

$$v^s(x) := \text{Re}\, v(x) = e^{-\alpha(\mu)x}p^s(x, \mu)$$

satisfies (3.1)-(3.3). It remains to show that $v^s(x)$ does not vanish identically: if it did, we repeat the arguments above for $\text{Im}\, v(x)$, which can then not vanish identically as we assumed that $v(x)$ is not the zero solution. Finally, Proposition 2.1 implies that $v^u(x) := \mathcal{R}v^s(-x)$ satisfies (3.1)-(3.3). $\square$
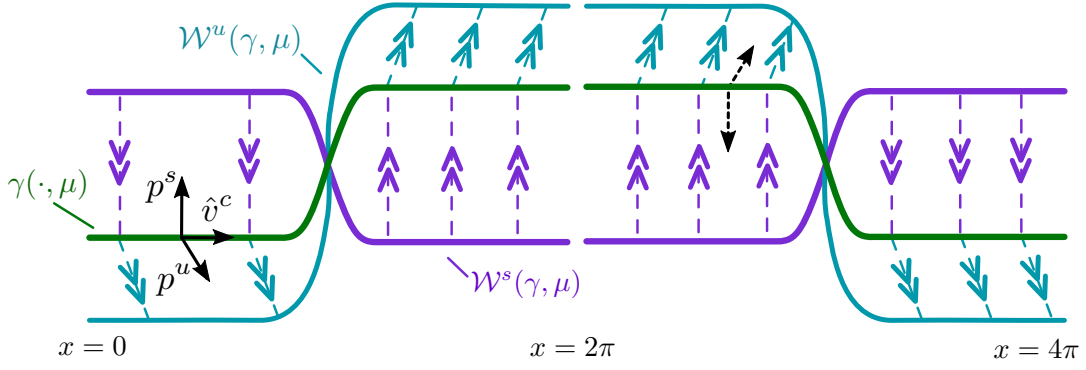
Figure 5: *Shown is an illustration of the stable and unstable manifolds of the periodic orbit γ in the nonorientable case: the vectors in black represent $p^s(x,\mu)$ and $p^u(x,\mu)$, and it is indicated how they change direction after 2π time units. Considering the phase in the interval $[0,4\pi]$ allows us to match the vector directions and visualize the stable and unstable manifolds of the periodic orbit as two Möbius bands glued together.*

Visually, we can see that (3.3) implies that the stable and unstable manifolds of the periodic orbit are Möbius bands as illustrated in Figures 5 and 6. When following a solution along the periodic orbit, the trajectory will be on the other side of the manifold after 2π time units due to the half-twist. This is reflected in the rotation of the vectors p^u and p^s as they move along the periodic orbit. In the following lemma, we will set up Fenichel coordinates near $\gamma(x,\mu)$ by gluing together two copies of the stable and unstable manifolds and consider the local coordinate describing the phase along γ to be 4π-periodic: see Figure 5.

Lemma 3.2. *Assume that Hypotheses 1-4 and 6 are met. There exists a $\delta > 0$, a smooth reversible change of coordinates near $\gamma(\cdot,\mu)$, and smooth real-valued functions h^c, h^s_j, and h^u_j for $j = 1,2$ with the following properties. Let $I = [-\delta, \delta]$ and $\mathbb{S}^1 := [0,4\pi]/\sim$, then (2.1) restricted to the zero energy level set is of the form*

$$
\begin{aligned}
\hat{v}^c_x &= 1 + h^c(\hat{v},\mu)\hat{v}^s\hat{v}^u \\
\hat{v}^s_x &= -[\alpha(\mu) + h^s_1(\hat{v},\mu)\hat{v}^s + h^s_2(\hat{v},\mu)\hat{v}^u]\hat{v}^s \\
\hat{v}^u_x &= [\alpha(\mu) + h^u_1(\hat{v},\mu)\hat{v}^s + h^u_2(\hat{v},\mu)\hat{v}^u]\hat{v}^u
\end{aligned}
\tag{3.4}
$$

for all $\mu \in J$ and $\hat{v} = (\hat{v}^c, \hat{v}^s, \hat{v}^u) \in \mathcal{V} := \mathbb{S}^1 \times I \times I/\sim$, where the equivalence relation $\sim$ in $\mathcal{V}$ is defined by

$$(\hat{v}^c, \hat{v}^s, \hat{v}^u) \sim (\hat{v}^c + 2\pi, -\hat{v}^s, -\hat{v}^u).$$

Furthermore, (3.4) is reversible with the reverser $\mathcal{R}$ acting on $\hat{v}$ as

$$\mathcal{R}\hat{v} = \mathcal{R}(\hat{v}^c, \hat{v}^s, \hat{v}^u) = (-\hat{v}^c, \hat{v}^u, \hat{v}^s). \tag{3.5}$$

Proof. The proof is analogous to the construction of Fenichel coordinates in [2, Lemma 2.1] via a transformation of the form

$$(\hat{v}^c, \hat{v}^s, \hat{v}^u) \in \mathbb{S}^1 \times I \times I \longmapsto \gamma(\hat{v}^c,\mu) + \hat{v}^s p^s(\hat{v}^c,\mu) + \hat{v}^u p^u(\hat{v}^c,\mu) + \text{h.o.t.}$$

except that we have $\hat{v}^c \in \mathbb{S}^1$. The nonorientability of the Floquet bundles is reflected in the fact that

$$\gamma(\hat{v}^c,\mu) + \hat{v}^s p^s(\hat{v}^c,\mu) + \hat{v}^u p^u(\hat{v}^c,\mu) = \gamma(\hat{v}^c + 2\pi,\mu) - \hat{v}^s p^s(\hat{v}^c + 2\pi,\mu) - \hat{v}^u p^u(\hat{v}^c + 2\pi,\mu).$$

Thus, under the above mapping, the points $(\hat{v}^c, \hat{v}^s, \hat{v}^u)$ and $(\hat{v}^c + 2\pi, -\hat{v}^s, -\hat{v}^u)$ would be sent to the same point in the neighborhood of the periodic orbit, and the equivalence relation in the definition of $\mathcal{V}$ reflects this symmetry. The action of the reverser on these coordinates can be checked using the relations $\mathcal{R}\gamma(x) = \gamma(-x)$ and $p^u(x,\mu) = \mathcal{R}p^s(-x,\mu)$. $\square$
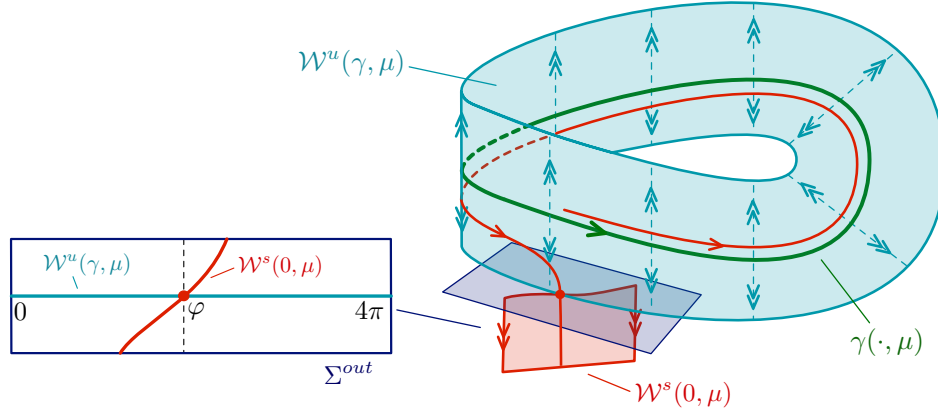
Figure 6: *Shown is a three-dimensional schematic of the gluing construction for systems with negative Floquet multipliers, where, for clarity, only $W^u(\gamma(x,\mu),\mu)$, the section Σ_{out}, and a heteroclinic orbit corresponding to an intersection of $W^s(0,\mu)$ with $W^u(\gamma(x,\mu),\mu)$ are shown. The setup is nearly identical to the orientable case, except that the phase coordinate $\varphi \in [0,4\pi]$ traverses γ twice.*

The equivalence relation on $\mathcal{V}$ implies that we can restrict our forthcoming analysis to $\hat{v}^s > 0$ and $\hat{v}^u > 0$. As explained in §2, the sets $\{\hat{v}: \hat{v}^s = 0\}$ and $\{\hat{v}: \hat{v}^c = \varphi, \hat{v}^s = 0\}$ correspond, respectively, to the unstable manifold of $\gamma(\cdot,\mu)$ and the strong unstable fibers $W^{uu}(\gamma(\varphi,\mu),\mu)$, and analogously for the stable manifold and the strong stable fibers. The variables $\hat{v}^c$ parametrize a double cover of the periodic orbit $\gamma(x,\mu)$. The sections Σ_{in} and Σ_{out} are defined via

$$\Sigma_{\mathrm{in}} = \mathbb{S}^1 \times \{\hat{v}^s = \delta\} \times I, \qquad \Sigma_{\mathrm{out}} = \mathbb{S}^1 \times I \times \{\hat{v}^u = \delta\}.$$

Our goal is to track solutions that enter a neighborhood of the periodic orbit near a back that lies in the intersection of the unstable manifold $W^u(0,\mu)$ of the equilibrium and a strong stable fiber $W^{ss}(\gamma(\varphi,\mu),\mu)$ of the periodic orbit and leave the neighborhood near a front that lies in the intersection of a strong unstable fiber $W^{uu}(\gamma(\varphi,\mu),\mu)$ and the stable manifold $W^s(0,\mu)$; see Figure 6. To capture the locations of backs and fronts, we define the set Γ via

$$\Gamma := \{(\varphi,\mu) \in \mathbb{S}^1 \times J : W^s(0,\mu) \cap W^{uu}(\gamma(\varphi,\mu),\mu) \cap \Sigma_{\mathrm{out}} \neq \emptyset\}. \tag{3.6}$$

Note that, compared to the orientable setup, the only change is that we use $\mathbb{S}^1 = [0,4\pi]/\sim$ instead of $S^1 = [0,2\pi]/\sim$. The following lemma shows how solutions that pass near the periodic orbit can be tracked.

Lemma 3.3. *There exist positive constants L_0 and η such that, for all $L > L_0$ and $\varphi \in \mathbb{S}^1$, there exists a unique solution $\hat{v}(x)$ of (3.4) that is defined for $x \in [-L, L]$ such that*

$$\hat{v}(-L) \in \Sigma_{\mathrm{in}}, \qquad \hat{v}(L) \in \Sigma_{\mathrm{out}}, \qquad \hat{v}^c(0) = \varphi, \qquad \hat{v}(x) \in \mathcal{V} \qquad \forall x \in [-L, L].$$

In addition, we have

$$\hat{v}(-L) = \left(\varphi - L + \mathrm{O}(\mathrm{e}^{-\eta L}), \delta, \delta\mathrm{e}^{-2\alpha(\mu)L}(1 + \mathrm{O}(\mathrm{e}^{-\eta L}))\right)$$

$$\hat{v}(L) = \left(\varphi + L + \mathrm{O}(\mathrm{e}^{-\eta L}), \delta\mathrm{e}^{-2\alpha(\mu)L}(1 + \mathrm{O}(\mathrm{e}^{-\eta L})), \delta\right) \tag{3.7}$$

$$\hat{v}(0) = \left(\varphi, \delta\mathrm{e}^{-\alpha(\mu)L}(1 + \mathrm{O}(\mathrm{e}^{-\eta L})), \delta\mathrm{e}^{-\alpha(\mu)L}(1 + \mathrm{O}(\mathrm{e}^{-\eta L}))\right).$$

The solution $\hat{v}(x)$ is smooth in (φ,μ,L), and the error estimates in (3.7) are differentiable. Moreover

$$\hat{v}(x,-\varphi) = \mathcal{R}\hat{v}(-x,\varphi) \tag{3.8}$$

for all φ and x. In particular, the solution $\hat{v}(x,\varphi)$ is $\mathcal{R}$-reversible, with $\hat{v}(0) \in \mathrm{Fix}\,\mathcal{R}$, if and only if $\varphi \in \{0, 2\pi\}$.

Proof. The proofs for existence and uniqueness of solutions as well as for obtaining (3.7) and (3.8) proceed as in [2, Lemma 3.1]. Finally, (3.8) implies that $\hat{v}(0) \in \mathrm{Fix}\,\mathcal{R}$ if and only if $\varphi = -\varphi$. Using that $-\varphi = 4\pi - \varphi$, we find that $\varphi = -\varphi$ if and only if $\varphi \in \{0, 2\pi\}$ as claimed. $\square$
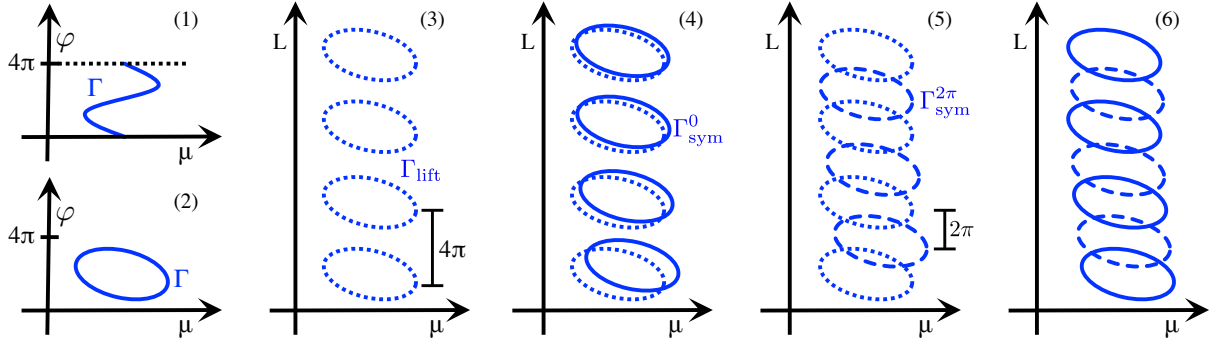
Figure 7: *Panels (1) and (2) show example sets Γ that are 1-loops and 0-loops, respectively. Panel (3) shows the set $\Gamma_{\text{lift}} = \Gamma + (0, 4\pi\mathbb{Z})$ (dotted) resulting from the 0-loop shown in panel (2), with the vertical axis variable φ replaced by L. Panels (4) and (5) show Γ_{lift} (dotted) together with the isolas Γ_{sym}^0 (solid) and $\Gamma_{\text{sym}}^{2\pi}$ (dashed), respectively, that correspond to symmetric pulses; see Lemma 4.1. Panel (6) shows the sets Γ_{sym}^0 (solid) and $\Gamma_{\text{sym}}^{2\pi}$ (dashed), whose union constitutes the full bifurcation diagram of symmetric pulses.*

4 Snaking and isolas for nonorientable Floquet bundles

In this section, we construct branches of symmetric and asymmetric pulses: our arguments will not depend on whether these branches are isolas or connected snaking branches. Since the case of orientable Floquet bundles has already been considered in [2], we restrict our analysis to the nonorientable case when the stable and unstable manifolds are topological Möbius bands.

We impose the following structural definition on the set Γ that describes heteroclinic connections between the origin and the periodic orbits:

Hypothesis 7. *There exists some smooth function $G : \mathbb{S}^1 \times I \times J \to \mathbb{R}$ such that $G(\varphi, \hat{v}^s, \mu) = 0$ if, and only if, $(\varphi, \hat{v}^s) \in W^s(0, \mu) \cap \Sigma_{\text{out}}$. In particular,*

$$\Gamma := \{(\varphi, \mu) \in \mathbb{S}^1 \times J : W^{uu}(\gamma(\varphi, \mu), \mu) \cap W^s(0, \mu) \cap \Sigma_{\text{out}} \neq \emptyset\} = \{(\varphi, \mu) \in \mathbb{S}^1 \times J : G(\varphi, 0, \mu) = 0\},$$

and we assume that $\Gamma \subset \mathbb{S}^1 \times \mathring{J}$ and that

$$\nabla_{(\varphi, \mu)} G(\varphi, 0, \mu) \neq 0 \qquad \forall (\varphi, \mu) \in \Gamma. \tag{4.1}$$

Throughout the remainder of this paper, we refer to one-dimensional manifolds that are diffeomorphic to circles as loops. In other words, loops are closed smooth curves that do not have self-intersections.

With this notation, the preceding hypothesis implies that Γ is the union of finitely many disjoint loops that do not intersect $\mathbb{S}^1 \times \partial J$. We pick one such loop and parametrize it by $(\varphi(s), \mu(s))$ with $s \in [0, 1]$, where we consider $\varphi(s)$ in the cover $\mathbb{R}$ of $\mathbb{S}^1$. Since we have $\varphi(0) = \varphi(1) \mod 4\pi$, and we trace out a loop, we have either (i) $\varphi(0) = \varphi(1)$ or (ii) $\varphi(0) = \varphi(1) \pm 4\pi$: we refer to the loop as a 0-loop in case (i) and a 1-loop in case (ii). Figure 7 shows examples of sets Γ that are 1-loops and 0-loops.

We now denote by $\Gamma_{\text{lift}} \subset \mathbb{R} \times \mathring{J}$ the preimage of Γ under the natural covering projection from $\mathbb{R} \times \mathring{J}$ to $\mathbb{S}^1 \times \mathring{J}$. Any 0-loop in Γ will be lifted to an infinite number of disjoint copies of the 0-loop, while a 1-loop will be lifted to an unbounded connected curve in Γ_{lift}. Below, we will show that the bifurcation curves of symmetric pulses will be close to Γ_{lift} so that we have snaking if Γ is a 1-loop, while the bifurcation diagram consists of isolas if Γ contains only 0-loops; see Figure 7 for an illustration.
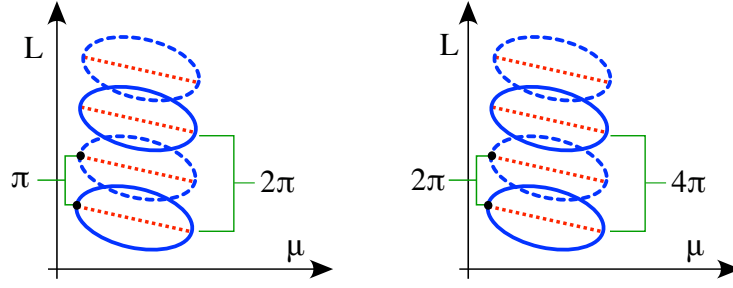
Figure 8: *Shown are sample bifurcation diagrams consisting of isolas in the orientable (left) and nonorientable (right) case: solid and dashed curves correspond to the branches Γ^0_{sym} and $\Gamma^{\varphi_0}_{\mathrm{sym}}$, respectively, of symmetric pulses with $\varphi_0 = \pi$ in the orientable and $\varphi_0 = 2\pi$ in the nonorientable case, while dotted curves correspond to branches of asymmetric pulses.*

4.1 Symmetric 1-pulses

In this section, we will construct symmetric solutions $\hat{v}(x)$ that are reversible homoclinic orbits to the equilibrium $u = 0$ and spend time $2L \gg 1$ near the periodic orbit $\gamma(\cdot, \mu)$. Here, by definition, a symmetric 1-pulse $\hat{v}(x)$ satisfies

$$\hat{v}(x) \in \mathcal{V} \quad \text{for} \quad x \in [-L, L]$$
$$\hat{v}(L) \in W^s(0, \mu) \cap \Sigma_{\mathrm{out}} \tag{4.2}$$
$$\hat{v}(0) \in \mathrm{Fix}(\mathcal{R})$$

for sufficiently large $L \gg 1$.

Lemma 4.1. *Assume that Hypotheses 1-4 and 6-7 are met. There exist an $\eta > 0$ and submanifolds $\Gamma^{\varphi_0}_{\mathrm{sym}} \subset \mathbb{R} \times J$ for $\varphi_0 = 0, 2\pi$ such that the following is true:*

1. *There is a symmetric 1-pulse of length $2L$ if, and only if, $(L, \mu) \in \Gamma^{\varphi_0}_{\mathrm{sym}}$ for $\varphi_0 = 0$ or $\varphi_0 = 2\pi$.*
2. *Fix $\varphi_0 = 0, 2\pi$, then the manifolds $\Gamma_{\mathrm{lift}} - (\varphi_0, 0)$ and $\Gamma^{\varphi_0}_{\mathrm{sym}}$ are, for each fixed $k \geq 2$, $\mathrm{O}(\mathrm{e}^{-\eta L})$-close to each other in the C^k-sense near any point $(L, \mu) \in \Gamma^{\varphi_0}_{\mathrm{sym}}$.*

The lemma implies that the bifurcation diagram of symmetric pulses is close to the set Γ_{lift} shifted by φ_0 upwards with $\varphi_0 \in \{0, 2\pi\}$; see Figure 8. In particular, we obtain snaking if Γ is a 1-loop; if Γ consists of 0-loops, the bifurcation diagram consists of isolas.

Proof. Lemma 3.3 implies that (4.2) is met if, and only if,

$$\hat{v}(L) = (\hat{v}^c(L, \varphi_0, \mu), \hat{v}^s(L, \varphi_0, \mu), \delta) \in W^s(0, \mu)$$

for $\varphi_0 \in \{0, 2\pi\}$, and Hypothesis 7 implies that this condition is equivalent to

$$G(\hat{v}^c(L, \varphi_0, \mu), \hat{v}^s(L, \varphi_0, \mu), \mu) = 0 \tag{4.3}$$

for any sufficiently large $L \gg 1$. Using again Lemma 3.3, we see that (4.3) becomes

$$G(L + \varphi_0 + \mathrm{O}(\mathrm{e}^{-\eta L}), \mathrm{O}(\mathrm{e}^{-\eta L}), \mu) = 0. \tag{4.4}$$

For each 0-loop in Γ, we parametrize the loop by 4π-periodic functions $(L(s), \mu(s))$ with $0 \leq s \leq 4\pi$ so that

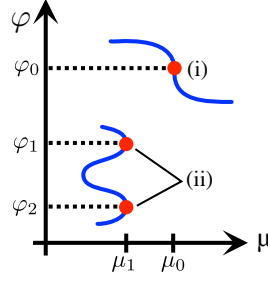$$\Gamma_{\mathrm{lift}} = \{(L(s) + 4\pi k, \mu(s)) : 0 \leq s \leq 4\pi, k \in \mathbb{N}\}.$$

Figure 9: *Shown are two curve segments inside a sample set* $\Gamma = \{(\mu, \varphi) : G(\varphi, 0, \mu) = 0\}$. *The upper segment violates Hypothesis 8(i) at the filled circle with label (i) at which* $G_\varphi(\varphi_0, 0, \mu_0) = G_{\varphi\varphi}(\varphi_0, 0, \mu_0) = 0$: Γ *is not locally a nondegenerate parabola near the point* (φ_0, μ_0) *that corresponds to the vertical tangent. The lower segment violates Hypothesis 8(ii) at the two filled circles with label (ii) at which two vertical tangents arise at the same value of* μ *so that* $G_\varphi(\varphi_j, 0, \mu_1) = 0$ *for* $j = 1, 2$.

If Γ is a 1-loop, we can parametrize Γ_{lift} by a curve $(L(s), \mu(s))$ with $s \geq 0$, where $(L(s + 4\pi), \mu(s + 4\pi)) = (L(s) + 4\pi, \mu(s))$ for all s. Next, let

$$n(s) := \frac{1}{|\nabla_{(\varphi,\mu)} G(L(s), 0, \mu(s))|} \nabla_{(\varphi,\mu)} G(L(s), 0, \mu(s))$$

and note that $n(s)$ is well defined and normal to Γ_{lift} for all s by Hypothesis 7. We now set

$$(L, \mu) = (L(s) - \varphi_0 + n_1(s)a, \mu(s) + n_2(s)a)$$

and note that there is an open interval I so that $(s, a) \in \mathbb{R} \times I$ parametrize a uniform neighborhood of Γ_{lift} in $\mathbb{R} \times J$. Let

$$F(s, a) := G(L + \varphi_0 + O(e^{-\eta L}), O(e^{-\eta L}), \mu) = G(L(s) + n_1(s)a, 0, \mu(s) + n_2(s)a) + O(e^{-\eta L(s)})$$

and we have

$$F(s, a) = O(|a| + e^{-\eta L(s)}), \qquad F_a(s, a) = 1 + O(|a| + e^{-\eta L(s)}).$$

In particular, we can solve $F(s, a) = 0$ uniquely for a for all sufficiently large s. The remaining claims now follow easily. $\qquad\square$

4.2 Asymmetric 1-pulses

Next, we focus on asymmetric (that is, not symmetric) 1-pulses, which, by definition, satisfy

$$\hat{v}(x) \in \mathcal{V} \quad \text{for} \quad x \in [-L, L]$$
$$\hat{v}(-L) \in W^u(0, \mu) \cap \Sigma_{\text{in}} \tag{4.5}$$
$$\hat{v}(L) \in W^s(0, \mu) \cap \Sigma_{\text{out}}$$

for sufficiently large $L \gg 1$. Throughout the remainder of this section, we assume that Hypotheses 1-4 and 6-7 are met. In addition, we assume the following nondegeneracy condition and refer to Figure 9 for a geometric interpretation:

Hypothesis 8. *If* $(\varphi, \mu) \in \Gamma$ *with* $G_\varphi(\varphi, 0, \mu) = 0$, *then (i)* $G_{\varphi\varphi}(\varphi, 0, \mu) \neq 0$ *and (ii)* $G_\varphi(\tilde{\varphi}, 0, \mu) \neq 0$ *for all* $(\tilde{\varphi}, \mu) \in \Gamma$ *with* $\tilde{\varphi} \neq \varphi$.

Lemma 3.3 and Hypothesis 7 imply that

$$\hat{v}(L) \in \Sigma_{\text{out}} \cap W^s(0, \mu) \iff G(\hat{v}^c(L, \varphi, \mu), \hat{v}^s(L, \varphi, \mu), \mu) = 0.$$

11

Applying the reverser to $\hat{v}(-L)$, and explicitly indicating the dependence of $\hat{v}(x, \varphi, \mu)$ on the variables (φ, μ), we conclude from Lemma 3.3 that $\hat{v}(-L, \varphi, \mu) \in \Sigma_{\text{in}} \cap W^u(0, \mu)$ if, and only if,

$$\hat{v}(L, -\varphi, \mu) \overset{(3.8)}{=} \mathcal{R}\hat{v}(-L, \varphi, \mu) \in \Sigma_{\text{out}} \cap W^s(0, \mu).$$

Thus, we see that 1-pulses that spend time $2L$ in $\mathcal{V}$ are in 1:1 correspondence with solutions (L, φ, μ) of the system

$$\mathcal{G}(L, \varphi, \mu) := \begin{pmatrix} G(\hat{v}^c(L, \varphi, \mu), \hat{v}^s(L, \varphi, \mu), \mu) \\ G(\hat{v}^c(L, -\varphi, \mu), \hat{v}^s(L, -\varphi, \mu), \mu) \end{pmatrix} = 0.$$

Denoting by κ the map given by $\kappa(u, v) = (v, u)$, we see that

$$\mathcal{G}(L, -\varphi, \mu) = \kappa\mathcal{G}(L, \varphi, \mu), \qquad \forall(L, \varphi, \mu)$$

so that $\mathcal{G}$ is $\mathbb{Z}_2$-equivariant with respect to this action: in particular, since $\varphi = -\varphi$ in $\mathbb{S}^1 = [0, 4\pi]/\sim$ precisely when $\varphi \in \{0, 2\pi\}$, we recover the symmetric 1-pulses constructed in Lemma 4.1 as solutions in the fixed-point space of this action. Next, setting

$$L = \ell + 4\pi n = \ell + \frac{4\pi}{\epsilon}, \qquad \ell \in \mathbb{S}^1, \quad \epsilon \in A := \{0\} \cup \left\{\frac{1}{n}; \ n \in \mathbb{N}\right\}$$

and using the expansions given in Lemma 3.3, we obtain

$$\mathcal{G}(L, \varphi, \mu) = \begin{pmatrix} G(L + \varphi + \mathrm{O}(\mathrm{e}^{-\eta L}), \mathrm{O}(\mathrm{e}^{-\eta L}), \mu) \\ G(L - \varphi + \mathrm{O}(\mathrm{e}^{-\eta L}), \mathrm{O}(\mathrm{e}^{-\eta L}), \mu) \end{pmatrix} = \begin{pmatrix} G(\ell + \varphi, 0, \mu) \\ G(\ell - \varphi, 0, \mu) \end{pmatrix} + \mathrm{O}(\mathrm{e}^{-\eta/\epsilon}). \tag{4.6}$$

We will now set $\epsilon = 0$ and construct asymmetric 1-pulses for the $\epsilon = 0$ case: our construction involves only the implicit function theorem and therefore extends immediately to the case $0 < \epsilon \ll 1$. due to the error estimates in (4.6). For simplicity, and with a slight abuse of notation, we write $G(\varphi, \mu) := G(\varphi, 0, \mu)$ from now on, thus omitting the second component, which is zero.

We therefore need to find $(\ell, \varphi, \mu) \in Q := \mathbb{S}^1 \times \mathbb{S}^1 \times J$ for which

$$\mathcal{G}(L, \varphi, \mu) = \begin{pmatrix} G(\ell + \varphi, \mu) \\ G(\ell - \varphi, \mu) \end{pmatrix} = 0,$$

which we write equivalently as

$$\tilde{\mathcal{G}}(\ell, \varphi, \mu) := \begin{pmatrix} G_1(\ell, \varphi, \mu) \\ G_2(\ell, \varphi, \mu) \end{pmatrix} := \begin{pmatrix} G(\ell + \varphi, \mu) + G(\ell - \varphi, \mu) \\ G(\ell + \varphi, \mu) - G(\ell - \varphi, \mu) \end{pmatrix} = 0 \tag{4.7}$$

and note that this system is $\mathbb{Z}_2$-symmetric under the action $\varphi \to -\varphi$ and $(G_1, G_2) \mapsto (G_1, -G_2)$. We begin by investigating pitchfork bifurcations from symmetric pulses.

Lemma 4.2. *Assume that Hypotheses 1-4 and 6-8 are met. Assume that $(\ell_0, \mu_0) \in \Gamma$ (so that $G(\ell_0, \mu_0) = 0$) with $G_\varphi(\ell_0, \mu_0) = 0$, then precisely two branches of asymmetric 1-pulses (related by $x \to -x$ symmetry) bifurcate from the symmetric 1-pulse corresponding to (ℓ_0, μ_0) in a pitchfork bifurcation.*

Proof. Since $G(\ell_0, \mu_0) = 0$, we have $\tilde{\mathcal{G}}(\ell_0, 0, \mu_0) = 0$, Furthermore, since $G_\varphi(\ell_0, \mu_0) = 0$, we find that

$$D\tilde{\mathcal{G}}(\ell_0, 0, \mu_0) = \begin{pmatrix} 2G_\varphi(\ell_0, \mu_0) & 0 & 2G_\mu(\ell_0, \mu_0) \\ 0 & 2G_\varphi(\ell_0, \mu_0) & 0 \end{pmatrix} = \begin{pmatrix} 0 & 0 & 2G_\mu(\ell_0, \mu_0) \\ 0 & 0 & 0 \end{pmatrix}.$$

Hypothesis 7 implies that $G_\mu(\ell_0, \mu_0) \neq 0$, and we can therefore solve $G_1(\ell, \varphi, \mu) = 0$ near $(\ell_0, 0, \mu_0)$ uniquely for $\mu = \mu_*(\ell, \varphi)$ as a function of (ℓ, φ). Writing $(\ell, \mu) = (\ell_0, \mu_0) + (\tilde{\ell}, \tilde{\mu})$ and using the $\mathbb{Z}_2$-symmetry that guarantees that G_2 is odd in φ, we can expand the function $G_2(\ell, \varphi, \mu)$ and find that

$$G_2(\ell, \varphi, \mu_*(\ell, \varphi)) = 2G_{\varphi\varphi}(\ell_0, \mu_0)\tilde{\ell}\varphi + \mathrm{O}(\varphi^3),$$

where $G_{\varphi\varphi}(\ell_0, \mu_0) \neq 0$ by Hypothesis 8(i). Dividing by φ, we can therefore solve $G_2(\ell, \varphi, \mu_*(\ell, \varphi)) = 0$ near $(\ell_0, 0, \mu_0)$ uniquely for ℓ as a function of φ. This proves the claim. $\qquad\square$
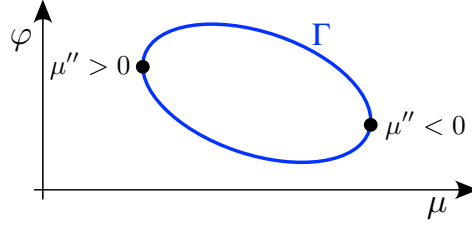
Figure 10: *We illustrate the curvature in the μ-direction at the points in Γ that correspond to pitchfork bifurcations.*

Next, let

$$\Lambda_{\mathrm{s}} := \{(\ell, \varphi, \mu) \in Q : \varphi = 0, G(\ell, \mu) = 0\}$$

$$\Lambda_{\mathrm{s}}^{\mathrm{bif}} := \{(\ell, \varphi, \mu) \in Q : \varphi = 0, \ G(\ell, \mu) = 0, \ G_{\varphi}(\ell, \mu) = 0, \}$$

$$\Lambda_{\mathrm{a}} := \{(\ell, \varphi, \mu) \in Q : \varphi \neq 0, \ G(\ell + \varphi, \mu) = 0, \ G(\ell - \varphi, \mu) = 0\}$$

to be the sets corresponding to symmetric 1-pulses, symmetric 1-pulses at pitchfork bifurcation points, and asymmetric 1-pulses. The following lemma characterizes the set Λ_{a} of asymmetric 1-pulses.

Lemma 4.3. *Assume that Hypotheses 1-4 and 6-8 are met. We have $\bar{\Lambda}_{\mathrm{a}} = \Lambda_{\mathrm{a}} \cup \Lambda_{\mathrm{s}}^{\mathrm{bif}}$, and $\bar{\Lambda}_{\mathrm{a}}$ consists of a finite union of smooth isolas (sets that are diffeomorphic to circles) and smooth curves with boundaries in $\Lambda_{\mathrm{s}}^{\mathrm{bif}}$.*

Proof. We already proved in Lemma 4.2 that precisely two branches of asymmetric 1-pulses emanate as smooth curves from each point in the discrete set $\Lambda_{\mathrm{s}}^{\mathrm{bif}}$.

Next, take any $(\ell, \varphi, \mu) \in \Gamma_{\mathrm{a}}$ with $\varphi \notin \{0, 2\pi\}$. In particular, $\mathcal{G}(\ell, \varphi, \mu) = 0$ and the associated Jacobian is given by

$$D\mathcal{G}(\ell, \varphi, \mu) = \begin{pmatrix} G_{\varphi}(\ell + \varphi, \mu) & G_{\varphi}(\ell + \varphi, \mu) & G_{\mu}(\ell + \varphi, \mu) \\ G_{\varphi}(\ell - \varphi, \mu) & -G_{\varphi}(\ell - \varphi, \mu) & G_{\mu}(\ell - \varphi, \mu) \end{pmatrix}. \tag{4.8}$$

It follows readily from Hypothesis 7 that the Jacobian has rank strictly less than two if and only if $G_{\varphi}(\ell \pm \varphi, \mu) = 0$. However, for $\varphi \notin \{0, 2\pi\}$ and $(\ell \pm \varphi, \mu) \in \Gamma$, this is ruled out by Hypothesis 8. Hence, the Jacobian has full rank, and the solution set of $\mathcal{G}(\ell, \varphi, \mu) = 0$ is given locally by a smooth curve.

Since Q is compact and zero is a regular value of $\mathcal{G}(\ell, \varphi, \mu)$ when we restrict it to a complement of a small neighborhood of Γ_{s}, this implies that Γ_{a} is the union of smooth isolas and of branches that begin and end in $\Lambda_{\mathrm{s}}^{\mathrm{bif}}$ as claimed. $\square$

Finally, we show that branches of asymmetric 1-pulses that emerge at pitchfork bifurcations begin and end at points in Γ of opposite curvature in μ. Take any element $(\varphi_0, \mu_0) \in \Gamma$ for which $G_{\varphi}(\varphi_0, \mu_0) = 0$. Since then $G_{\mu}(\varphi_0, \mu_0) \neq 0$ by Hypothesis 7, we can parametrize Γ locally near (φ_0, μ_0) as $\mu = \mu_*(\varphi)$ so that $G(\varphi, \mu_*(\varphi)) \equiv 0$. Taking derivatives, we find that

$$\mathrm{sign}\, \mu''(\varphi_0) = -\,\mathrm{sign}\, (G_{\mu}(\varphi_0, \mu_0)G_{\varphi\varphi}(\varphi_0, \mu_0)), \tag{4.9}$$

where the right-hand side is not zero due to Hypothesis 8. Note also that these signs are independent of the specific parametrization.

Lemma 4.4. *Assume that Hypotheses 1-4 and 6-8 are met. The branches of asymmetric 1-pulses described in Lemma 4.2 begin and end at points in $\Lambda_{\mathrm{s}}^{\mathrm{bif}}$ at which μ'' has opposite sign.*

Proof. Pick a branch of asymmetric 1-pulses that begins and ends at pitchfork bifurcation points and parametrize the branch $(\ell, \varphi, \mu)(s)$ by $s \in [0, 1]$ so that $(\ell, \varphi, \mu)'(s)$ never vanishes. It follows from the analysis in Lemma 4.2 that $(\ell, \mu)'(s) = 0$ and $\varphi'(s) \neq 0$ for $s = 0, 1$. Noting that the rows of the Jacobian in (4.8) are linearly independent and that the vector $(\ell, \varphi, \mu)'(s)$ lies in the null space of this Jacobian, we conclude that scalar product of $(\ell, \varphi, \mu)'(s)$ with the cross product of the two rows of the Jacobian in (4.8) has constant nonzero sign. Expanding the cross product of
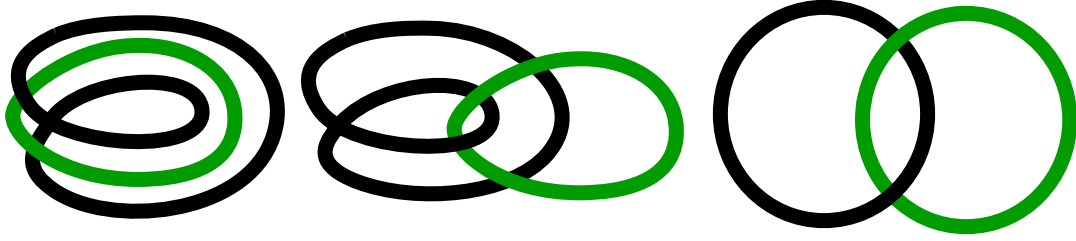
13

Figure 11: *From left to right: the boundary curve of a Möbius band (black) and its central circle (green) can be deformed to a pair of circles that have linking number one [1].*

the two rows at $s = 0, 1$ we see that this scalar product is given by $G_\mu(\ell(0), \mu(0))G_{\varphi\varphi}(\ell(0), \mu(0))\varphi'(0)^2$ at s=0 and by $-G_\mu(\ell(1), \mu(1))G_{\varphi\varphi}(\ell(1), \mu(1))\varphi'(1)^2$ at $s = 1$. This implies that the signs of $G_\mu G_{\varphi\varphi}$ at the start and end points of the branch must be opposites of each other, and inspecting (4.9) completes the proof. $\qquad\square$

5 Topological barriers to snaking

In the previous section, we proved that the structure of the set

$$\Gamma = \{(\varphi, \mu) \in \mathcal{P} \times J : W^s(0, \mu) \cap W^{uu}(\gamma(\varphi, \mu), \mu) \cap \Sigma_{\mathrm{out}} \neq \emptyset\}, \qquad \mathcal{P} := \begin{cases} [0, 2\pi]/\sim & \text{orientable manifolds} \\ [0, 4\pi]/\sim & \text{nonorientable manifolds} \end{cases}$$

determines whether the bifurcation diagram of symmetric pulses consists of an unbounded snaking branch or of the union of isolas. Specifically, if Hypothesis 7 is met, then snaking occurs if Γ is a 1-loop in $\mathcal{P} \times J$. In this section, we discuss topological barriers that prevent Γ from being a 1-loop and that therefore preclude snaking to occur.

5.1 Motivation

We begin with outlining our initial intuition and motivation for topological barriers to snaking. Consider a generic differential equation in $\mathbb{R}^3$ (we imagine that this system represents the differential equation inside the level set $H^{-1}(0)$ of the conserved quantity H) and neglect dependence on parameters in the following arguments. Assume that this system has a hyperbolic periodic orbit γ and suppose furthermore that the invariant manifold $W^u(\gamma)$ of the periodic orbit γ is a Möbius band. In this case, the section Σ_{out} is a cylinder with one full twist: Indeed, the boundary of the Möbius band $W^u(\gamma)$ is a loop $\mathfrak{w}$ that winds twice around the meridian circle given by the periodic orbit γ (see also Figure 11). The section Σ_{out} intersects $W^u(\gamma)$ along the entire loop $\mathfrak{w}$ and makes a half twist each time it traverses the periodic orbit once, thus ending up with one full twist since $\mathfrak{w}$ traverses γ twice.

To obtain snaking in the nonorientable case, we need that the intersection of the stable manifold $W^s(0)$ of the equilibrium with the section Σ_{out} forms a loop $\mathfrak{g}$ along γ: in contrast to the orientable case, the loop $\mathfrak{g}$ now winds twice around γ as it traverses Σ_{out} along the boundary loop $\mathfrak{w}$. The key is now that the loops $\mathfrak{g}$ and γ link, where linking is defined as follows: The fundamental group of $\mathbb{R}^3 \setminus \gamma$ is given by $\mathbb{Z}$, and each loop $\mathfrak{g}$ in $\mathbb{R}^3$ that does not intersect γ can therefore be mapped to a unique integer in $\mathbb{Z}$ via its equivalence class in the fundamental group $\mathbb{R}^3 \setminus \gamma$. This integer is the linking number of the pair $(\gamma, \mathfrak{g})$. Figure 11 shows that the linking number of $(\gamma, \mathfrak{g})$ is not zero. On the other hand, since $\mathfrak{g} \subset W^s(0)$, we can deform $\mathfrak{g}$ inside $\mathbb{R}^3 \setminus \gamma$ to a small neighborhood of the origin, thus unlinking the loops γ and $\mathfrak{g}$. This is impossible as the linking number is a homotopy invariant for homotopies in $\mathbb{R}^3 \setminus \gamma$. Therefore, linking of loops can create the topological barrier to snaking. We note that by similar arguments, one expects that additional twists in the Floquet bundles of γ (see, e.g. Figure 1) generate similar topological barriers due to linking in $\mathbb{R}^3$.

However, the above notion of linking rests on the fact that the fundamental group of $\mathbb{R}^3 \setminus \gamma$ is $\mathbb{Z}$. We need to consider the case where $\mathbb{E} = H^{-1}(0)$, and this set is a three-dimensional manifold (if we remove critical points of H) whose

topology can be arbitrarily complex. In particular, it is not clear how linking arguments can be used in this context, or whether there is an intrinsic notion of twisting within $H^{-1}(0)$. For this reason, we therefore focus on arguments involving the fundamental group.

5.2   Barriers in reversible, conservative systems

We focus on reversible, conservative systems in $\mathbb{R}^4$ that satisfy Hypotheses 1-4. Instead of using linking, we will utilize homotopies of loops. We will make the following assumptions on the conserved quantity $H : \mathbb{R}^4 \times J \to \mathbb{R}$.

Hypothesis 9. *We assume that $H : \mathbb{R}^4 \times J \to \mathbb{R}$ satisfies the following assumptions:*

1. $H_u(u, \mu) = 0$ *if, and only if, $f(u, \mu) = 0$.*
2. *If $H_u(u, \mu) = 0$, then the Hessian $H_{uu}(u, \mu)$ is invertible.*
3. *There is a bounded set $K \subset \mathbb{R}^4$ such that $H_u(u, \mu) \neq 0$ for all $(u, \mu) \notin K \times J$.*

We say that (u, μ) is a critical point of H if $H_u(u, \mu) = 0$. The preceding hypothesis implies that the set of critical points is diffeomorphic to the cross product of a finite set with J and in $1 : 1$ correspondence with the set of equilibria. Furthermore, each critical point is nondegenerate, and we can therefore use the Morse lemma to characterize the level sets of H near each equilibrium for each fixed μ. We now define

$$\mathcal{C} := \{(u, \mu) \in \mathbb{R}^4 \times J : H_u(u, \mu) = 0\}, \qquad \mathcal{C}_\mu := \mathcal{C} \cap (\mathbb{R}^4 \times \{\mu\}) \subset \mathbb{R}^4,$$
$$\mathcal{E} := H^{-1}(0) \setminus U_\delta(\mathcal{C}) \subset \mathbb{R}^4 \times J, \qquad \mathcal{E}_\mu := \mathcal{E} \cap (\mathbb{R}^4 \times \{\mu\}) \subset \mathbb{R}^4,$$

where $0 < \delta \ll 1$ is so small that the Morse lemma applies in the δ-neighborhood of each equilibrium in $\mathcal{C}$. Note that $\mathcal{E}$ is a four-dimensional manifold with boundary given by $\partial U_\delta(\mathcal{C})$ and, similarly, each slice $\mathcal{E}_\mu$ is a three-dimensional manifold with boundary given by $\partial U_\delta(\mathcal{C}_\mu)$. Finally, let $\mathfrak{w}_\mu$ be the loop that corresponds to the intersection $W^u(\gamma(\cdot, \mu), \mu) \cap \Sigma_{\text{out}}$ of the local unstable manifold of the periodic orbit $\gamma(\cdot, \mu)$ with the boundary of the tubular Fenichel neighborhood.

Theorem 5.1. *Assume that Hypotheses 1-4, 7, and 9 are met. If $\mathfrak{w}_\mu$ cannot be deformed continuously to a curve in $\partial U_\delta(0)$ inside $\mathcal{E}_\mu \setminus \{\gamma(\cdot, \mu)\}$ for some $\mu \in \mathring{J}$, then Γ cannot be a 1-loop and snaking is precluded in this situation.*

Proof. Hypothesis 9 implies that the manifolds $\mathcal{E}_\mu$ with $\mu \in J$ are diffeomorphic to each other. We fix some $\mu_0 \in \mathring{J}$ and denote by $\mathcal{T}_\mu$ the Fenichel tubular neighborhoods $\mathcal{T}_\mu$ introduced in §2-3. These coordinates provide an isotopy of

$$\bigcup_{\mu \in J} \mathcal{T}_\mu \times \{\mu\} \subset \mathcal{E}$$

with $\mathcal{T}_{\mu_0} \times J$ that maps each periodic orbit $\gamma(\cdot, \mu)$ onto $\gamma(\cdot, \mu_0)$. We can then use the isotopy extension theorem [5, Theorem 1.4 in Chapter 8] to extend this isotopy to an isotopy of $\mathcal{E}$ to $\mathcal{E}_{\mu_0} \times J$: we remark that the openness assumption needed in the isotopy extension theorem is automatically met as the tubular Fenichel neighborhoods $\mathcal{T}_\mu$ do not intersect $\partial \mathcal{E}_\mu$. We can therefore work in the framework where $\mathcal{E} = \mathcal{E}_{\mu_0} \times J$ and $\gamma(\cdot, \mu) = \gamma(\cdot, \mu_0)$ for all $\mu \in J$.

We now argue by contraposition: we assume that Γ is a 1-loop and need to show that $\mathfrak{w}_{\mu_0}$ can be deformed to a curve in $\partial U_\delta(0)$ in $\mathcal{E}_{\mu_0} \setminus \{\gamma(\cdot, \mu_0)\}$.

We identify $\Gamma \subset \mathcal{P} \times J$ with the one-dimensional manifold

$$\mathfrak{g} := \{(u, \mu) \in \mathcal{E} = \mathcal{E}_{\mu_0} \times J : u \in W^s(0, \mu) \cap W^{uu}(\gamma(\varphi, \mu), \mu) \cap \Sigma_{\text{out}} \text{ for some } (\varphi, \mu) \in \Gamma\}.$$

Note that $\mathfrak{g} \subset \mathcal{E}_{\mu_0} \setminus \{\gamma(\cdot, \mu_0)\} \times J$ and, using Fenichel coordinates, we can deform the loop $\mathfrak{w}_{\mu_0}$ into the loop $\mathfrak{g}$ in $(\mathcal{E}_{\mu_0} \setminus \{\gamma(\cdot, \mu_0)\}) \times J$. Let $\Phi_t(u, \mu)$ be the flow of the differential equation $\dot{u} = f(u, \mu)$ in the coordinates $\mathcal{E} = \mathcal{E}_{\mu_0} \times J$ given by the isotopy and note that the set $\{\gamma(\cdot, \mu_0)\}$ is invariant under $\Phi_t(\cdot, \mu)$ for each μ. We define the differentiable

function $h(t,\theta) := \Phi_t(u_\theta, \mu_\theta)$, where $t \geq 0$ and $\theta \in S^1$. Note that $h(0,\theta)$ parametrizes the projection of $\mathfrak{g}$ onto $\mathcal{E}_{\mu_0}$ and that $h(t,\theta) \in \mathcal{E}_{\mu_0} \setminus \{\gamma(\cdot, \mu_0)\}$ for all (t,θ). Furthermore, since $(u_\theta, \mu_\theta) \in W^s(0, \mu_\theta)$ for all $\theta \in S^1$, we see that $h(t,\theta) \to 0$ as $t \to \infty$ uniformly in θ. Possibly after introducing a new μ-dependent norm, we can assume that $W^s_{\mathrm{loc}}(0, \mu) \cap \partial U_\delta(0)$ is transverse to the flow for all $\mu \in J$ so that $W^s_{\mathrm{loc}}(0, \mu) \cap U_\delta(0)$ is forward invariant for all μ. In particular, for each $\theta \in S^1$, there is a unique $T_\theta > 0$ such that $h(T_\theta, \theta) \in \partial U_\delta(0)$, and T_θ is continuous in θ. Redefining h as the continuous function

$$h(t,\theta) := \Phi_{\min(t, T_\theta)}(u_\theta, \mu_\theta)$$

and setting $T := \max_\theta T_\theta$ shows that $h(T,\theta) \in \partial U_\delta(0)$ for each θ. The composition of the homotopy from $\mathfrak{w}_{\mu_0}$ to the projection of $\mathfrak{g}$ into $\mathcal{E}_{\mu_0}$ combined with the homotopy $h(t,\theta)$ of the the projection of $\mathfrak{g}$ into $\mathcal{E}_{\mu_0}$ into $\partial U_\delta(0)$ provides the desired homotopy of $\mathfrak{w}_{\mu_0}$ into $\partial U_\delta(0)$: note that we avoid $\{\gamma(\cdot, \mu_0)\}$ through both homotopies as needed. This completes the proof of the theorem. $\qquad\square$

Remark 5.2. *To connect our theorem to the discussion in §5.1, assume that $\mathcal{E} = \mathbb{R}^3$ and that $\gamma(\cdot)$ is a hyperbolic periodic orbit in $\mathcal{E}$ with nonorientable invariant manifolds. It follows, in particular, that $W^u_{\mathrm{loc}}(\gamma(\cdot)) \cap U_\delta(\gamma(\cdot))$ is a loop that cannot be contracted to a point in $\mathcal{E} \setminus \{\gamma(\cdot)\}$, and we conclude from Theorem 5.1 that Γ cannot be a 1-loop. We remark that this scenario was considered in [6], where it was assumed that Γ is a 1-loop: our results show that this case cannot occur.*

6 Application to the Swift–Hohenberg equation

In this section, we apply our results to the Swift–Hohenberg equation, and we present numerical computations that illustrate our results. Specifically, we identify a regime in the Swift–Hohenberg equation in which there are both orientable and nonorientable periodic orbits. We also show that the nonorientable periodic orbits cannot lead to snaking branches but only to isolas: this finding is again corroborated using numerical computations.

We consider the steady-state equation

$$-(1 + \partial_x^2)^2 U - \mu U + U^2 - U^3 = 0, \qquad x \in \mathbb{R}, \tag{6.1}$$

associated with the Swift–Hohenberg equation, where we have set $\nu = 2$. Bifurcating from the rest state $U = 0$ at $\mu = 0$ is a family of stationary periodic orbits with zero energy shown in Figure 12. The nontrivial Floquet multipliers of these solutions are shown in the insets: they lie on the unit circle at onset, then become real and negative, then switch back to the unit circle before finally becoming real and positive after crossing the fold. In particular, for a range of values of the parameter μ, there exist two periodic orbits with zero energy, one with positive Floquet multipliers, and one with negative Floquet multipliers.

Recall that (6.1) has the conserved quantity

$$H(u, \mu) = u_1^2 + u_1 u_3 - \frac{1}{2} u_2^2 + \frac{(1+\mu)}{2} u_0^2 - \frac{2}{3} u_0^3 + \frac{1}{4} u_0^4, \qquad u = (u_0, u_1, u_2, u_3) = (U, U_x, U_{xx}, U_{xxx}).$$

For a fixed small $\delta > 0$, we set

$$\mathcal{E}_\mu := \{u \in \mathbb{R}^4 : |u| \geq \delta, \ H(u, \mu) = 0\}.$$

We then have the following result on the structure of the zero-energy level sets $\mathcal{E}_\mu$ of H.

Lemma 6.1. *For each $\mu \geq 0$, the set $\mathcal{E}_\mu$ is diffeomorphic to $S^1 \times S^1 \times [\delta, \infty)$ with fundamental group $\pi_1(\mathcal{E}_\mu) = \mathbb{Z} \times \mathbb{Z}$.*

Proof. We need to characterize the set of $u \in \mathbb{R}^4$ for which $H(u, \mu) = 0$. Using the expression for H, we obtain

$$0 = u_1^2 + u_1 u_3 - \frac{1}{2} u_2^2 + \frac{(1+\mu)}{2} u_0^2 - \frac{2}{3} u_0^3 + \frac{1}{4} u_0^4 = \left(u_1 + \frac{1}{2} u_3\right)^2 - \frac{1}{4} u_3^2 - \frac{1}{2} u_2^2 + \frac{(1+\mu)}{2} u_0^2 - \frac{2}{3} u_0^3 + \frac{1}{4} u_0^4. \tag{6.2}$$
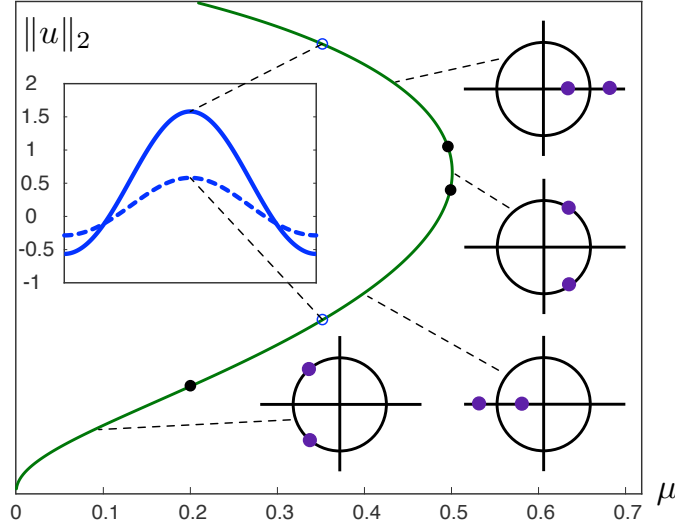
Figure 12: *Shown is the family of periodic orbits with zero energy emerging from $\mu = 0$ in the Swift–Hohenberg equation (1.1) with nontrivial Floquet multipliers indicated in the insets. Note that, for a range of values of μ, there exist both orientable (positive Floquet multipliers) and nonorientable (negative Floquet multipliers) periodic orbits. At the value of $\mu = 0.35$, the profiles of the periodic orbits are shown: the orientable and nonorientable orbits are shown in solid and dashed blue, respectively.*

Setting

$$\tilde{u}_0 := u_0 \sqrt{\frac{(1+\mu)}{2} - \frac{2}{3}u_0 + \frac{1}{4}u_0^2}, \qquad \tilde{u}_1 := u_1 + \frac{1}{2}u_3, \qquad \tilde{u}_2 := \frac{1}{\sqrt{2}}u_2, \qquad \tilde{u}_3 = \frac{1}{2}u_3, \qquad (6.3)$$

where we note that the function $u_0 \mapsto \tilde{u}_0$ is a diffeomorphism for $\mu \geq 0$, we see that the equation describing $\mathcal{E}_\mu$ becomes

$$\tilde{u}_0^2 + \tilde{u}_1^2 = \tilde{u}_2^2 + \tilde{u}_3^2.$$

Thus, $(\tilde{u}_0, \tilde{u}_1)$ and $(\tilde{u}_2, \tilde{u}_3)$ live on circles of the same radius $r \geq \delta$, which proves the claim. $\qquad\square$

Next, we calculate the element in the fundamental group of $\mathcal{E}_\mu$ associated with the periodic orbits found in Figure 12.

Lemma 6.2. *Assume that $\gamma(\cdot, s)$ is a continuous family of periodic orbits of (6.1) for $\mu = \mu(s) \geq 0$ with $s > 0$ so that (i) $H(\gamma(\cdot, s), \mu(s)) = 0$, (ii) $\gamma(\cdot, s) \to 0$ and $\mu(s) \to 0$ as $s \to 0$, and (iii) the Floquet multipliers of $\gamma(\cdot, s)$ at one has multiplicity two for all $s > 0$. Then the element $[\gamma(\cdot, s)]$ corresponding to the periodic orbits in the fundamental group $\pi_1(\mathcal{E}_\mu(s)) \cong \mathbb{Z} \times \mathbb{Z}$ of $\mathcal{E}_{\mu(s)}$ is given by $(-1, -1)$ using the coordinates (6.3).*

Proof. The periodic orbits that bifurcate from $u = 0$ when $\mu = 0$ and lie in the zero energy level set are of the form

$$u = \epsilon(\cos x, -\sin x, -\cos x, \sin x) + \mathrm{O}(\epsilon^2)$$

for $0 < \epsilon \ll 1$. Using the coordinates (6.3), we find that

$$\tilde{u} = \epsilon \left(\frac{1}{\sqrt{2}}\cos x, \frac{-1}{2}\sin x, \frac{-1}{\sqrt{2}}\cos x, \frac{1}{2}\sin x \right) + \mathrm{O}(\epsilon^2)$$

and we see that both $(\tilde{u}_0, \tilde{u}_1)$ and $(\tilde{u}_2, \tilde{u}_3)$ traverse a circle clockwise precisely once as x varies through one period. This proves the claim for $0 < \mu \ll 1$. Our assumption on the multiplicity of the trivial Floquet multiplier at one allows us to continue the branch of periodic orbits in a locally unique way as fixed points of appropriate Poincare maps. This, together with the fact that the topological type of $\mathcal{E}_\mu$ does not change by Lemma 6.1, completes the proof. $\qquad\square$
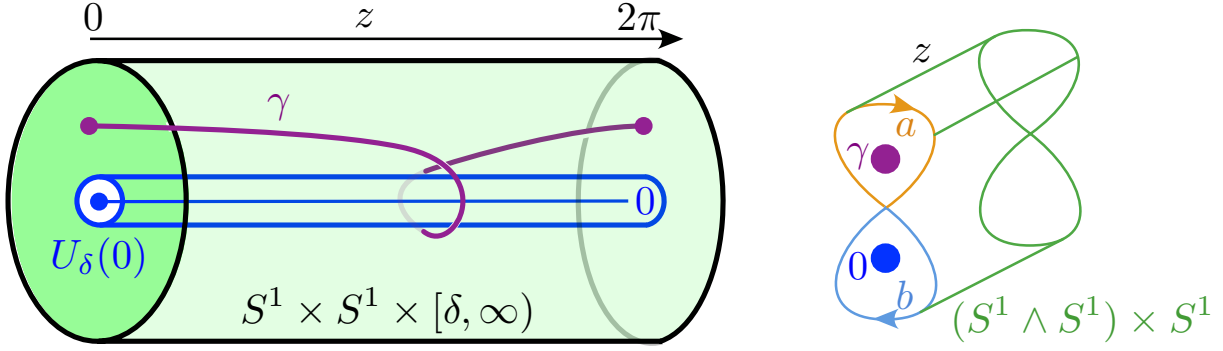
Figure 13: *Shown are the location of the periodic orbit γ in $\mathcal{E}_\mu$ (left panel) and the generators a, b, z of the deformation retract $(S^1 \vee S^1) \times S^1$ of $\mathcal{M}$ that form a basis of the fundamental group $\pi_1(\mathcal{M})$.*

Next, we use Theorem 5.1 to show that symmetric pulses that connect to the nonorientable periodic orbits shown in Figure 12 cannot snake.

Proposition 6.3. *If, in addition to the hypotheses made in Lemma 6.2, the nontrivial Floquet multipliers of $\gamma(\cdot, s)$ are negative for some $s > 0$, then the loop $\mathfrak{w} := W_{\mathrm{loc}}^u(\gamma(\cdot, s), \mu(s)) \cap U_\delta(\gamma(\cdot, s))$ cannot be deformed to a curve in $U_\delta(0)$ inside $\mathcal{E}_{\mu(s)} \setminus \{\gamma(\cdot, s)\}$. In particular, Theorem 5.1 precludes snaking involving these periodic orbits.*

Proof. Consider the manifold $\mathcal{M} := \mathcal{E}_\mu \setminus (U_\delta(0) \cup U_\delta(\gamma))$. As illustrated in Figure 13, $\mathcal{M}$ deformation retracts onto $(S^1 \vee S^1) \times S^1$ and the fundamental group $\pi_1(\mathcal{M})$ is therefore given by $\pi_1(\mathcal{M}) = (\mathbb{Z} * \mathbb{Z}) \times \mathbb{Z}$ and each element in $\pi_1(\mathcal{M})$ can be written as (w, n), where w is an arbitrary word in the loops a and b that surround γ and 0, respectively, and $n \in \mathbb{Z}$ measures the winding number in the z-direction; see Figure 13 for these definitions. In particular, any curve that lies completely in $\partial U_\delta(0) \subset \mathcal{M}$ is represented by (b^{m_1}, n_1) where $m_1, n_1 \in \mathbb{Z}$. If γ is nonorientable, then the loop $\mathfrak{w} \in \partial U_\delta(\gamma) \subset \mathcal{M}$ that corresponds to the intersection of the local unstable manifold $W_{\mathrm{loc}}^u(\gamma)$ with $\partial U_\delta(\gamma)$ corresponds to an element of the form (a^{m_2}, n_2) in $\pi_1(\mathcal{M})$, where $m_2 \neq 0$ is odd as $\mathfrak{w}$ links with γ in $U_\delta(\gamma)$ since the unstable manifold is nonorientable. In particular, $\mathfrak{w}$ cannot be deformed in $\mathcal{M}$ to an element in $\partial U_\delta(0)$. This proves the result. $\qquad\square$

Remark 6.4. *From the proof of Proposition 6.3, we see that there is in fact a barrier to snaking whenever $m_2 \neq 0$ in the element (a^{m_2}, n_2) of $\pi_1(\mathcal{M})$ corresponding to the intersection of the local unstable manifold $W_{\mathrm{loc}}^u(\gamma)$ with the boundary $\partial U_\delta(\gamma)$ of a tubular neighborhood of the periodic orbit γ. The integer m_2 can be thought of as measuring the degree to which $W_{\mathrm{loc}}^u(\gamma)$ twists relative to the ambient manifold $\mathcal{M}$ while traversing γ, and hence in the case of Swift-Hohenberg, we think of $W_{\mathrm{loc}}^u(\gamma)$ as being twisted whenever $m_2 \neq 0$. Proposition 6.3 demonstrates that this is always the case when $W_{\mathrm{loc}}^u(\gamma)$ is nonorientable.*

Finally, we report on numerical computations of the bifurcation diagrams of stationary localized patterns associated with the orientable and nonorientable periodic orbits shown in Figure 12. First, we consider the orientable periodic orbits associated with the upper branch of the curve of periodic solutions and, using AUTO, find snaking branches of symmetric solutions: the resulting bifurcation diagram is shown in Figure 14. Note that the solutions near $\mu = 0.35$ exhibit a plateau of roll patterns whose amplitude matches that of the orientable periodic orbit shown in the inset of Figure 12 for $\mu = 0.35$.

Next, we computed the localized solutions associated with the nonorientable periodic orbits associated with the lower branch in Figure 12. The results are shown in Figure 15: localized symmetric solutions exist for arbitrary length, but these are now found to form a family of disjoint isolas rather than a connected snaking branch, in line with the statements proved in Proposition 6.3. A comparison of the amplitude of the roll patterns for $\mu = 0.35$ with that of the periodic orbits shown in Figure 12 confirms that the roll pattern matches the nonorientable periodic orbit.
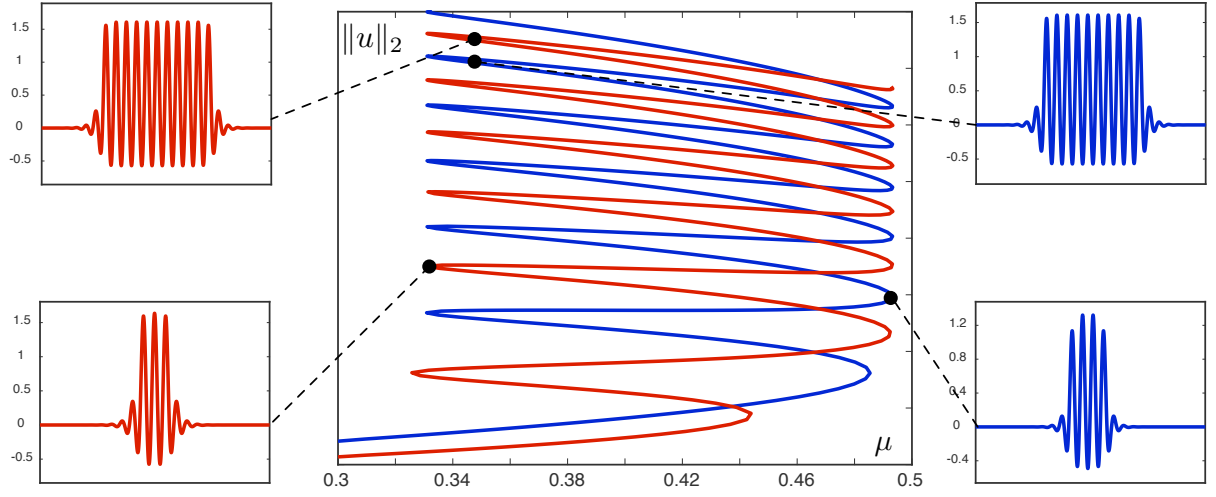
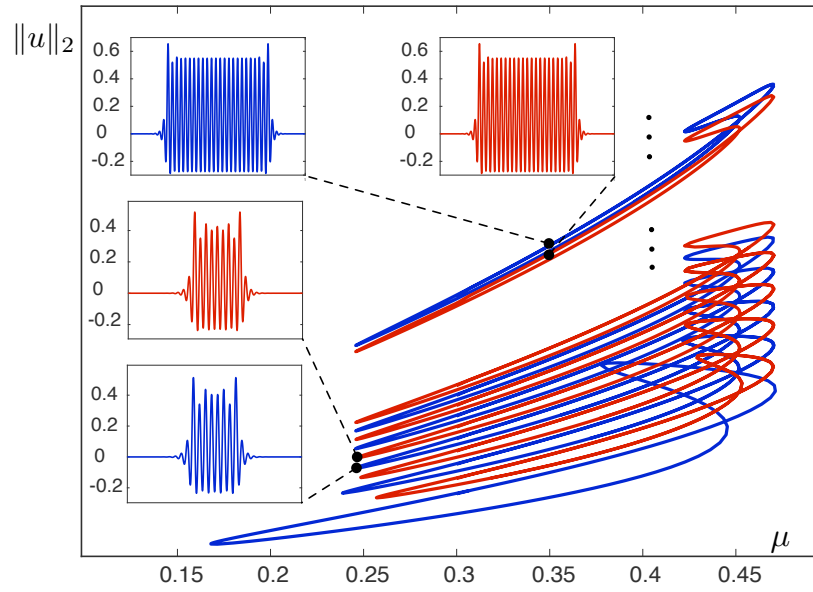Figure 14: *Snaking of orientable localized rolls in the Swift–Hohenberg equation.*

Figure 15: *Isolas of nonorientable localized rolls in the Swift–Hohenberg equation.*

7 Discussion

In this paper, we analyzed localized roll solutions in four-dimensional conservative, reversible dynamical systems that admit periodic orbits whose stable and unstable manifolds may be orientable or nonorientable, thus extending previous work [2] in which the orientable case was considered. The orientability of these manifolds is related to the sign of the nontrivial Floquet multipliers associated with the periodic orbit, and the structure of the set Γ of intersections between the unstable manifold of the periodic orbits and the stable manifold of the rest state are proved to be key to understanding the global structure of the associated bifurcation diagrams.

Generically, the set Γ is a one-dimensional curve that lives on a cylinder. We developed topological criteria that result in different bifurcation diagrams: informally, in order to have snaking of symmetric pulses, Γ should take the form of a nontrivial loop on this cylinder, whilst, in order to see isolas of symmetric pulses, Γ should take the form of a null-homotopic loop. We made these arguments precise and proved the existence of isolas and snaking under these conditions in §4 and also constructed branches of asymmetric pulses, proceeding in a similar manner as in previous work [2]. We emphasize that these arguments extend in a straightforward way to higher-dimensional systems.

As already mentioned, in order for snaking to occur, Γ needs to correspond to a loop $\mathfrak{g}$ that can be deformed to the loop $\mathfrak{w}$ that corresponds to the intersection of the unstable manifold of the periodic orbit with the boundary of a fixed neighborhood of the periodic orbit. Since $\mathfrak{g}$ lives in the stable manifold of the homogeneous rest state, it can be deformed to a loop that lies entirely near the origin without passing through the periodic orbit. Thus, the same needs to be true for the loop $\mathfrak{w}$, which results in a topological condition for $\mathfrak{w}$ that is necessary for snaking. We applied these results to the Swift–Hohenberg equation and showed that nonorientable unstable manifolds of roll patterns that arise from bifurcations from the rest state cannot satisfy this topological condition, thus precluding snaking. We also note that more general twisting which violates this topological condition can be defined relative to the fundamental group of the phase space in Swift–Hohenberg, regardless of orientability. Our numerical computations of bifurcation diagrams for rolls with orientable and nonorientable unstable manifolds corroborated these findings as they showed that bifurcation diagrams of localized patterns associated with an orientable periodic orbit exhibit snaking, while those associated with a nonorientable periodic orbit break up into a sequence of isolas.

We note that the topological barrier we elucidated here is also present in three-dimensional non-conservative systems such as the one considered in [6], and we expect that snaking is impossible in such a system when the nontrivial Floquet multipliers of the periodic orbit are negative.

Our topological argument regarding the nonexistence of snaking relies heavily on the structure of the fundamental group of the energy level set minus the periodic orbit. One advantage of using the fundamental group instead of the linking argument that we mentioned in §5.1 is that linking of loops is traditionally defined in three-dimensional Euclidean space, while the fundamental group is defined regardless of the dimension or topology of the underlying manifold. It is not clear to us though whether there are topological barriers in higher dimensions or whether snaking can happen regardless of the orientability of the unstable manifolds.

The reason why nonorientability is an obstruction for snaking in the Swift–Hohenberg equation is that the periodic orbit can be deformed to the neighborhood of the origin as the periodic orbits bifurcates from the origin. It would be interesting to see whether there are examples where the periodic orbit forms a loop that cannot be deformed to a neighborhood of the homogeneous rest state: in this case, snaking could not occur if the invariant manifolds of the periodic orbit are orientable, while nonorientability may make them deformable to the origin.

References

[1] Colin C. Adams. *The knot book*. American Mathematical Society, Providence, RI, 2004.

[2] Margaret Beck, Jürgen Knobloch, David J. B. Lloyd, Björn Sandstede, and Thomas Wagenknecht. Snakes, ladders, and isolas of localized patterns. *SIAM J. Math. Anal.*, 41(3):936–972, 2009.

[3] John Burke and Edgar Knobloch. Localized states in the generalized Swift-Hohenberg equation. *Phys. Rev. E (3)*, 73(5):056211, 15, 2006.

[4] P. Coullet, C. Riera, and C. Tresser. Stable static localised structures in one dimension. *Rhysical Review Letters*, 84:3069–3072, 2000.

[5] Morris W. Hirsch. *Differential topology*, volume 33 of *Graduate Texts in Mathematics*. Springer-Verlag, New York, 1994.

[6] Jürgen Knobloch, Thorsten Rieß, and Martin Vielitz. Nonreversible homoclinic snaking. *Dyn. Syst.*, 26(3):335–365, 2011.

[7] Jürgen Knobloch and Martin Vielitz. Non-conservative perturbations of homoclinic snaking scenarios. *J. Differential Equations*, 260(1):517–566, 2016.

[8] Jürgen Knobloch, Martin Vielitz, and Thomas Wagenknecht. Non-reversible perturbations of homoclinic snaking scenarios. *Nonlinearity*, 25(12):3469–3485, 2012.

[9] Y. Pomeau. Front motion, metastability, and subcritical bifurcations in hydrodynamics. *Phys. D*, 130:73–104, 1999.

[10] Björn Sandstede and Yancong Xu. Snakes and isolas in non-reversible conservative systems. *Dyn. Syst.*, 27(3):317–329, 2012.

[11] P. D. Woods and A. R. Champneys. Heteroclinic tangles and homoclinic snaking in the unfolding of a degenerate reversible Hamiltonian-Hopf bifurcation. *Phys. D*, 129(3-4):147–170, 1999.